In-flight data acquisition and flight testing for system identification of flapping-wing MAVs

Caetano, J. V.; Armanini, S. F.; Karásek, M.

DOI
10.1109/ICUAS.2017.7991452

Publication date
2017

Document Version
Accepted author manuscript

Published in
2017 International Conference on Unmanned Aircraft Systems, ICUAS 2017

In-flight data acquisition and flight testing for system identification of flapping-wing MAVs

J.V. Caetano*†, S. F. Armanini†, M. Karásek†
*Portuguese Air Force Research Center, Portuguese Air Force Academy, Sintra, Portugal
†Section of Control and Simulation, Faculty of Aerospace Engineering, Delft University of Technology, Delft, The Netherlands
Corresponding author: jvcaetano@academiafa.edu.pt; DelFly research contact: microuav@gmail.com

***Abstract*—Although flapping-wing micro aerial vehicles have become a hot topic in academia, the knowledge we have of these systems, their force generation mechanisms and dynamics is still limited. Recent technological advances have allowed for the development of free flight test setups using on-board sensors and external tracking systems, for system identification purposes. Nevertheless, there is still little knowledge about the system requirements, as well as on how to perform free flight test experiments, and process the collected data. The present article presents the guidelines for flapping-wing micro aerial vehicle free flight testing. In particular, it gathers information produced by different studies and provides the best practices for the proper system dimensioning, system setup, on-board sensors, maneuver input design, error analyses and data post-processing, for the reconstruction of the forces and moments that act during free flight of a flapping-wing robot, for system identification and modeling purposes. Furthermore, this article compares the results obtained using external optical position tracking systems with on-board and external sensor fusion, and provides suitable solutions and methods for data fusion and force reconstruction.**

I. INTRODUCTION

Flapping-Wing Micro Aerial Vehicles (FWMAV) have become a hot topic in research and development studies. This boom, witnessed in the past 10 years, is motivated by the technological developments that have allowed for the miniaturization of the systems, as well as by the developments made in the on-board and off-board sensors that allow for testing and modeling of the systems.

While the first studies on flapping wings (late twentieth century) focused on understanding the kinematics, aerodynamics and dynamics of flapping-wing species [1]–[3] later research focused on the study of independent flapping-wing systems [4]–[6]. Recent developments have allowed for the recent studies to use technologically advanced FWMAV and external test infrastructures for the study and modeling of the aerodynamics and dynamic behavior, in both free flight [7]–[12] and wind tunnel [13] experiments.

If, on the one hand, wind tunnel experimental setups are especially suited for fundamental studies on flapping flight, e.g., local aerodynamic and wake analysis [14], on the other hand these setups limit the effectiveness of dynamic system identification, due to the tethering of the FWMAV. Conversely, free flight experimental setups allow for the reconstruction of the flight dynamics and, consequently, the development of both aerodynamic and dynamic models, as well as flight control strategies.

Nevertheless, free flight experimental strategies are difficult to perform, as they require: *i)* flight-capable robots; *ii)* expensive external tracking facilities, that have sufficient resolution and size for accurate data recording; *iii)* suitable flight test maneuver input design; *iv)* some kind of on-board sensors or control, e.g., inertial measurement unit, radio control unit or autopilot; *v)* extensive data processing and error analysis.

The present article addresses these specific requirements and presents recommendations and guidelines for the collection and respective post-processing of data obtained from free flight experimental techniques, based on prior testing made with different systems and vehicles across literature [9], [15]–[22]. In particular, it collects the best practices to perform free flight tests, compares different external tracking systems, compares them to on-board inertial measurement unit logging, and presents flight path reconstruction methods to accurately reconstruct and quantify the flight states and acting forces, while minimizing the error and uncertainty in the data. Different options of internal and on-board sensors are presented, and the effects of sensor resolution and numerical differentiation are thoroughly analyzed.

It is structured as follows: Section II presents the requirements of the external tracking systems, the marker placement, the flight path reconstruction process, and the procedure for error analysis; Section III discusses data acquisition using on-board sensors, focusing on the positioning and mounting of these sensors and on the reconstruction of forces from these data; Section IV outlines and evaluates a method to combine on-board and off-board measurements, involving time synchronization and sensor fusion; Section V discusses the most relevant flight testing procedures, particularly focusing on input design for flapping-wig system identification; Section VI ends the article with a summary of the main conclusions.

II. OPTICAL MOTION TRACKING

A. Requirements of the Flight Arena and Optical Tracking System

There is a considerable number of commercial systems that are able to record the position, in time, of markers in 3D

space, e.g., Vicon, OptiTrack. The specifications and setup of the tracking system must be selected to meet the requirements of the analyses that are to be performed. In particular, the system should: *i)* be able to track very small and light markers (or LEDs) to guarantee the least impact of the added mass on the flapping robot; *ii)* be able to deliver sub-millimeter accuracy at the average speed of flight, especially during maneuvers – see Sec. II-E ; *iii)* have a sampling frequency at least five times greater than the flapping frequency of the system, in order to be able to capture sub-flap time-resolved forces – see Sec. II-F; *iv)* have a tracking volume suitable for the type of dynamic identification of interest[1], i.e., should one want to perform forward flight system identification, the largest measurable dimension of the flight chamber should allow for a straight flight at the desired speed, lasting longer than the expected time of oscillation.

B. Marker placement

Given the small platform size and the restricting weight limitations, retro-reflective markers are typically used for the tracking of FWMAV (Fig. 1a). These can have spherical or flat shapes—the former, despite being heavier, allow for higher marker accuracy as they provide an almost constant reflective area to the tracking system. Therefore, such 3D markers are recommended for rigid body structure definition, to guarantee that the collected data can be reconstructed. For moving parts, e.g., the wings, circular flat shape tape-like markers are recommended. Worth noting that the resolution of the tracking system will dictate the size of the marker. As an example, 1mm accuracy was obtained with markers of 1cm of diameter using a Vicon system [19].

Alternatively, the FWMAV may also be equipped with IR-LED diodes (e.g., OP280PS by OpTEK Technology) as active markers (Fig. 1b) [21]. Although this solution increases the power consumption of the system (around 75 mW per marker), the active markers greatly improve the tracking reliability and, most importantly, can be used for time synchronization. For example, one of the markers can be turned on at the beginning of a pre-programmed control actuator sequence used for system identifications. It can also be used to synchronize the motion tracking data with an on-board logged data set or with telemetry (cf. Sec. IV). Due to their small size ($\approx$ 3 x 3 mm) and mass (below 50 mg), the IR LEDs can be placed even at the wing-tip or at a carbon rod extension of the rudder and elevator (see the detail in Fig. 1b), which allows for recording of the flapping angle and the deflection of the control surfaces with an increased accuracy.

In terms of positioning on the robot, there are two requirements: *i)* guarantee that there is no symmetry plane formed by the markers, to avoid loss of orientation; *ii)* the proximity of the markers, and therefore, the number of markers, should be selected to avoid marker swap or fusion .

[1]In the case of hovering FWMAV, or identification and control around hover conditions, this factor should not be a limitation

(a) Retro-reflective markers placed on the robot

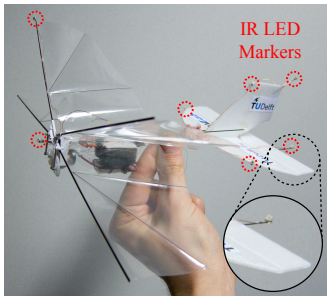

(b) Robot equipped with active IR-LED markers, which can also be used for time synchronization.

Fig. 1. Types of markers recommended for optical tracking.

C. Flight Path Reconstruction

Flight path reconstruction techniques [9], [17], [23] are recommended for the full reconstruction of the states of the robot during the maneuvers. For the case of tracking systems that do not provide the body orientation, we recommend performing direct-cosines transformation between the Inertial $(\boldsymbol{X_I}, \boldsymbol{Y_I}, \boldsymbol{Z_I})$ and the Body $(\boldsymbol{X_b}, \boldsymbol{Y_b}, \boldsymbol{Z_b})$ reference frames (see Eq. 1[2]), and corresponding each matrix entry to the "3-2-1" rotation matrix (see Eq.2[3]), to determine the rotation matrices between frames. This step allows one to determine the *i)* attitude of the ornithopter; *ii)* control surface deflection; and *iii)* wing position and flap angle.

While different strategies are available for the reconstruction of the flight velocity and acceleration, we recommend that these are computed using three-point central difference differentiation scheme, when the frequency of the motion tracking system is at least five times greater than the highest frequency one wants to capture—more details are given in Sec. II-F.

$$\mathcal{R}_{bI} = \begin{bmatrix} i_{b_x} & i_{b_y} & i_{b_z} \\ j_{b_x} & j_{b_y} & j_{b_z} \\ k_{b_x} & k_{b_y} & k_{b_z} \end{bmatrix} \tag{1}$$

$$\mathcal{R}_{bI} = \begin{bmatrix} c\theta c\psi & c\theta s\psi & -s\theta \\ c\phi c\theta c\psi - c\phi c\psi & c\phi c\psi + s\phi s\theta s\psi & s\phi c\theta \\ s\phi s\psi + c\phi s\theta c\psi & s\phi c\psi - c\phi s\theta s\psi & c\phi c\theta \end{bmatrix} \tag{2}$$

D. Characterizing the Random Error

The cyclic nature of flapping flight complicates the quantification of the measurement and process errors. As a baseline, three a priori tests are recommended: *i)* data collection of the position data of the markers on the robot, with the final marker configuration using a static (non-moving) robot at different locations in the room – this can be used to determine the highest precision and lowest process noise threshold; *ii)* same as *i)* with the wings flapping, e.g., robot held in place on a pedestal while the wings flap; *iii)* (if possible) flight tests

[2]$(i_{b_x}, i_{b_y}, i_{b_z})$ represents the coordinates of the unit vectors $(\boldsymbol{x}_b, \boldsymbol{y}_b, \boldsymbol{z}_b)$ in the Inertial reference frame.

[3]s and c correspond, respectively, to sin and cos functions.

around the room with a fixed-wing non oscillating aircraft with a similar size as the FWMAV – allows for streak (motion blur), velocity and maneuver effects to be quantified, yet without the cyclic harmonic information of a flapping system.

The following step is to determine the nature of the random error (noise). Should this error be found to be non-random or biased, the reconstructed information must be treated and used with caution A first step is to hypothetically model the error in the position as a zero-mean, independent and identically distributed (IID) random variable [15], here $v(k) \in IID(0, \sigma^2)$, and confirm the assumption using the following method:

$$\hat{x}(k) = x(k) + v(k) \tag{3}$$

$\hat{x}(k)$ the estimated position; $x(k)$ the real position;

Analyze the frequency spectrum (e.g., recurring to a power spectral density analysis) of the position data of the static and fixed-wing flight test mentioned above (*ii)* and *iii)*). If this spectrum does not present cyclic peaks or correlations, as presented in Fig. 2, the residual of the measured position can be calculated using:

$$\epsilon(k) = \hat{x}(k) - \hat{x}_{f_c}(k) \tag{4}$$

where $\hat{x}_{f_c}(k)$ is the state filtered at a cut-off frequency f_c, by applying a zero-phase lag low-pass filter [4].

To confirm the hypothesis of an IID process, the autocorrelation function of the residual, here $\rho_\epsilon(k)$ (Eq. 5), should be within the 95% confidence criterion, bounded by $\pm 1.96/\sqrt{n}$ (n is the number of samples), as in [24]:

$$\rho(l) = \frac{\gamma(l)}{\gamma(0)} \tag{5}$$

with $\gamma(l)$ representing the autocovariance function at the lag l defined as:

$$\gamma(l) = cov[\epsilon(t), \epsilon(t+l)] = E[(\epsilon(t) - \mu)(\epsilon(t+l) - \mu)] \tag{6}$$

where μ is the expected value of the process.

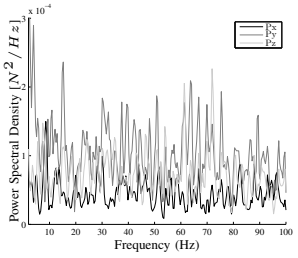

(a) Power spectral density plot of the position measurements of the markers.

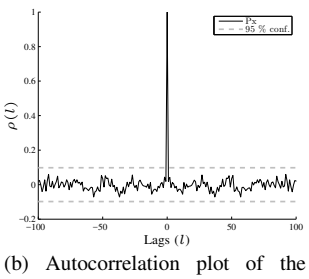

(b) Autocorrelation plot of the residuals determined with Eq. 4, with f_c=1Hz..

Fig. 2. Frequency spectrum and autocorrelation of the residuals in a static test.

[4]e.g., implemented in Matlab with the command `design(fdesignhandle,'cheby2','MatchExactly','stopband')`.

A careful selection of the number of samples and auto-covariance lags must be performed to guarantee statistical proof, using the final flight data with the flapping-wing robot. This is done by selecting samples that contain more than fifty points ($N > 50$); lags are $L \leq \frac{N}{4}$ [25]. N and L have to be determined for each system, and selected to minimize the correlation of the residuals. For a 200Hz sampling and 12Hz flapping-wing robot, N was found to be 400 and L equal to 100 samples [19].

Now that the number of samples and lags have been determined and that the system noise has been concluded to be IID (cf. Fig.2), one must repeat the assessment of the autocorrelation using the position data collected during the flight of the flapping-wing robot. The first step is to determine the filtering frequency to be used for the computation of the residuals (Eq. 4). Furthermore, this step is important to determine the filtering frequency of the low-pass zero-lag filter that will be used to filter the position data *i)* because low-pass filtering is important to avoid excessive noise magnification when performing time or frequency differentiation; and *ii)* to determine the filtering frequency that maximizes the number of autocorrelation points within the 95% confidence bounds.

As a result, different filtering frequencies must be used to compute Eqs. 5 and 6. Following the example of the 200Hz sampling frequency system mentioned above, Fig. 3b presents the analysis for one flight test, using 400 samples and lag of 100. As observed, the percentage of points within the confidence bounds is smaller than 95% for all filtering frequencies (Fig. 3a). This is justified by correlations that occur at lag times that correspond to the flapping frequency (see Fig. 3b) – for this specific case, high autocorrelation values above the 95% bound ($\pm 1.96/\sqrt{n}$ dashed line) occur at lag times that are multiples of $recordfreq(Hz)/flapfreq.(Hz) = 16$. As a result, should this percentage of points under the confidence bound be close to 95%, for any reasonable filtering frequency (i.e., higher than the flapping frequency and preferably lower than one fourth of the sampling frequency), this result confirms the hypothesis of IID random error on the position measurements.

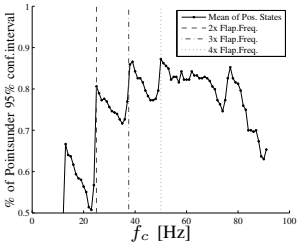

(a) Mean of the percentage of points of the position states (P_x, P_y, P_z) under 95% confidence interval, at different cut-off frequencies f_c.

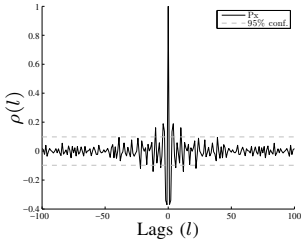

(b) Autocorrelation ($\rho(l)$) plot for the residuals of the position in $\boldsymbol{x}_I$ (P_x) computed using Eq. 4, with f_c=40Hz.

Fig. 3. Example of Autocorrelation of the residuals of the position measurements for one of the free-flight tests.

This analysis leads to two important results: a) the verifica-

tion of the IID random error; b) the determination of filtering frequency that leads to lower noise autocorrelation.

E. Quantifying the Uncertainty in the Measured States

Typically, the small size of the robots limits the number of markers placed on the platform, making it challenging to have more than one set of markers defining each structure. As a result, it is difficult to assess the uncertainty, and therefore, the precision of the position measurements. To assess this value we recommend performing a comparison between the physical distance between the geometric center of the markers/LED placed on the robot measured, e.g., using a caliper[5], and the same relative distance measured using the optical tracking system, written in equation form as:

$$Error_t = \overline{Mark1Mark2}_{tracker_t} - \overline{Mark1Mark2}_{real} \quad (7)$$

which results in an array of the size of t that contains the distance between the physical and the measured distances between two markers. Assuming the errors in the position of the markers are uncorrelated, exhibiting equal standard deviation, the uncertainty in the position can be determined using the standard deviation of the error [26]:

$$\sigma_{Mark1} = \sigma_{Mark2} = \frac{\sigma_{Error}}{2} \quad (8)$$

Furthermore, the uncertainty in the attitude angles (ϕ, θ, ψ) can be assessed using:

$$\sigma_\phi = \sigma_\theta = \sigma_\psi = \arctan\left(\frac{\sigma_{Mark1} + \sigma_{Mark2}}{\overline{Mark1Mark2}_{real}}\right) \quad (9)$$

This methodology allows for the determination of the uncertainty affecting the position of all markers, and accounts for the loss of precision due to velocity, acceleration and attitude rate of change, mentioned above.

F. Error Propagation and Effects of Numerical Differentiation

A discrete time differentiation of the position data is recommended to determine the velocity and acceleration states. Although this method promotes the magnification of the noise in the signal, it avoids adding (or removing) dynamics to the states, when compared to other methods, e.g., spline fitting prior to differentiation. Among the discrete time differentiation strategies, we suggest using three point (kernel) central-difference differentiation, as it does not introduce any lag in the new states, and reduces the uncertainty magnification by two when compared to two point (forward or backward) differentiation methods. Moreover, it gains over five point (Lagrange) methods, as it conserves the system dynamics and still results in a smaller uncertainty magnification.

[5]note that this measurement is not exact and is used to assess if the measurement of the tracking system has a bias, serving as ground truth of the distance between the markers.

The uncertainty in the differentiated states can be determined using the output of Eq. 8 in the following error propagation expression [27], with $f = f(x, y, ...)$:

$$\sigma_f^2 = \sigma_x^2 \left(\frac{\partial f}{\partial x}\right)^2 + \sigma_y^2 \left(\frac{\partial f}{\partial y}\right)^2 + ... + 2\sigma_{xy}^2 \left(\frac{\partial f}{\partial x}\right)\left(\frac{\partial f}{\partial y}\right) + ... \quad (10)$$

If the errors in the states are shown to be uncorrelated (see Sec. II-D), the cross-variance terms in the previous equation can be suppressed.

Nevertheless, the three point central difference method introduces low-pass filtering in the differentiated states. As a result, this differentiation method is advised only when the sampling frequency is at least five times the frequency of the fastest dynamic mode. An example is presented in Fig. 4, which compares the attenuation of the signal for two (forward) and three point central difference methods for a tracking sampling frequency of 200Hz [6].

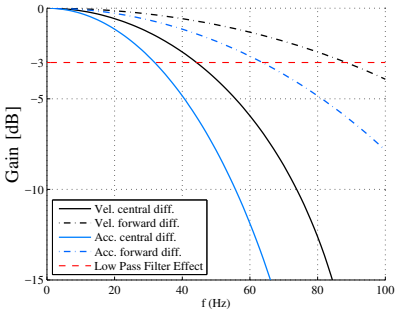

Fig. 4. Attenuation in the calculated velocities and accelerations using two point forward and three point central difference schemes. Red dashed line indicates attenuation of -3 dB, equivalent to a half amplitude low-pass filter effect.

Should the frequency of the tracking system not meet the requirement of being five times higher than the fastest dynamic motion of interest, differentiation in the frequency domain is recommended. This can be performed, e.g., to determine the accelerations from velocities obtained from time differentiation, if the sampling frequency is two to three times higher than the flapping frequency:

$$a = \mathcal{F}^{-1}[(\mathcal{F}(V)/F_s) \times j\omega \times F_s] \quad (11)$$

where a, $\mathcal{F}$, $\mathcal{F}^{-1}$, F_s are the acceleration, Fourier Transform, inverse Fourier transform and tracking sampling frequency respectively; ω is the frequency being differentiated and j is the imaginary unit. This method, however, introduces a considerable amount of noise noise at high frequencies, when compared to time differentiation methods. Fig. 5 presents the power spectral density of the acceleration along the normal body axis (z_b) using time and frequency differentiation methods.

[6]detailed information about the mathematics can be found in [19], [28].

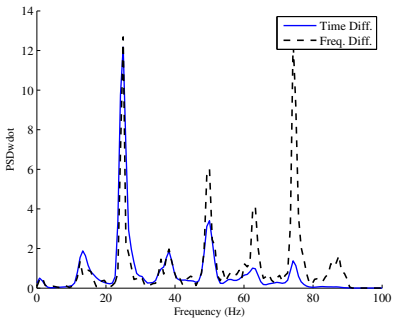

Fig. 5. Power spectral density of the linear acceleration along z_b axis of the flying robot, at 0.3m/s, F_s = 200Hz and Flapping Freq = 13.3Hz.

III. On-board sensor data

For a detailed analysis of the sub-flap effects, the flapping-wing MAV may be equipped with a MEMS Inertial Measurement Unit (IMU), consisting of a 3-axis accelerometer and a 3-axis gyroscope. Compared to the external motion tracking system data, such an on-board sensor typically provides data with higher temporal resolution (Invensense MPU 6000 - 1000Hz / 8000 Hz) and measures directly the body accelerations and angular rates, which are the dominant terms in the equations of motion (translational part) and only single differentiation (which has been shown to have low-pass filtering effect in the previous section) is necessary to get the rate derivatives for the rotational equations.

The data can either be logged on-board or sent via telemetry to the ground station, if a link of sufficient bandwidth is available. In our tests, on-board logging with sampling rates of up to 1024 Hz was achieved with a 2.8 g Lisa/S autopilot board, running Paparazzi UAV system, and a microSD card [21]. Lightweight WiFi modules, such as the 0.5 g ESP8266 ESP-09 with UART communication, may be used with the same autopilot for high speed telemetry.

A. IMU placement and mounting

Ideally, the IMU should be placed close to the CG so that the measured accelerations $\mathbf{a_{IMU}}$ can be used directly for in-flight force estimation. If, due to design constraints, this is not possible, a transformation to CG is necessary:

$$\mathbf{a_{CG}} = \mathbf{a_{IMU}} + \left(\Omega^2 + \dot{\Omega}\right)(\mathbf{r_{CG}} - \mathbf{r_{IMU}}), \qquad (12)$$

where Ω represents the tensor of angular velocities measured by the gyroscope, $\dot{\Omega}$ is its derivation, computed numerically, e.g. using three-point central difference scheme, and $\mathbf{r_{IMU}}$ and $\mathbf{r_{CG}}$ are the position vectors of IMU and CG in body-fixed frame, respectively.

As evident from the build materials, the FWMAV fuselage is not rigid and is prone to structural vibrations. An effect of these vibrations on force balance measurements has been reported during clamped wind tunnel experiments [19]. Structural vibrations will also be present in free flight; while IMU placement close to the nodes of dominant modes is desirable, it is often not sufficient. High frequency vibrations, excited by the flapping wings, can easily be larger than the sensing range of the MEMS IMUs (MPU 6000: $\pm$16 g / $\pm$2000 deg/s) and cause sensor saturation. This can be prevented by using a soft mount acting as a vibration isolator. Its design should be chosen carefully, so that the low frequency signals remain unaffected. A common practice is to mount the lightweight IMU board together with a (relatively heavy) battery, which allows for using a stiffer mount. An example of such a soft mount made of PU foam blocks is presented in Fig. 6.

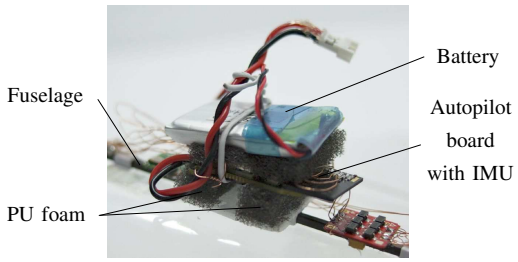

Fig. 6. An example of a soft mount of the autopilot board preventing the IMU saturation.

1) Other Important Data: The on-board data set may not be restricted only to IMU data. Data from other on-board sensors, as well as actuator commands, can be logged or sent via telemetry. Some propulsion motor speed controllers can provide rpm feedback (e.g. the MI-3A ESC with a customized BL Heli firmware), which provides a measure of flapping frequency and a measurement of instantaneous wing position, due to varying motor load over the flapping cycle. A log of actuator commands is indispensable when evaluating the trim curves or the control effectiveness of various control devices.

2) Attitude and force estimation: Body attitude can be estimated by transforming the angular rates vector to the derivatives of Euler angles and by their subsequent integration. Because of accumulation of gyroscope biases and measurement errors during the integration process, the resulting drift needs to be compensated by the accelerometer data. This is typically done with a complementary filter, e.g., [29]. A more elaborate approach is to employ an Extended Kalman Filter, which can also be used for fusion with the motion tracking system data (further developed in Sec. IV).

Assuming the FWMAV is a rigid body, the IMU data can also be used to estimate the forces acting on the body during flight, using the Euler's equation of motion:

$$\mathbf{F} = m\mathbf{a_{CG}} \qquad (13)$$

$$\mathbf{M} = \mathbf{I}\dot{\boldsymbol{\omega}} + \boldsymbol{\omega} \times (\mathbf{I}\boldsymbol{\omega}). \qquad (14)$$

where $\mathbf{a_{CG}}$ are the accelerations transformed to the CG, $\boldsymbol{\omega}$ and $\dot{\boldsymbol{\omega}}$ the angular rates and their derivatives, estimated by differentiation of the gyro readings, and $\mathbf{I}$ is the inertia matrix.

Fig. 7 shows a comparison between the in-flight forces estimated with motion-tracking based data (recorded at 120

Hz, presented in blue) and with IMU data (recorded at 512 Hz, presented in red). As a reference, wind-tunnel forces measured with a sensitive load cell (ATI Nano17-Ti) for similar flight conditions are also shown (magenta). The test conditions were described in [21] and [22].

The lack of detail in the pure motion tracking estimates is visible, which is caused by the lower sampling rates and the low-pass filtering effect of the necessary double differentiation of the position data. On the contrary, the IMU data carry also higher frequencies and the force estimates are very close to the wind tunnel measurements.

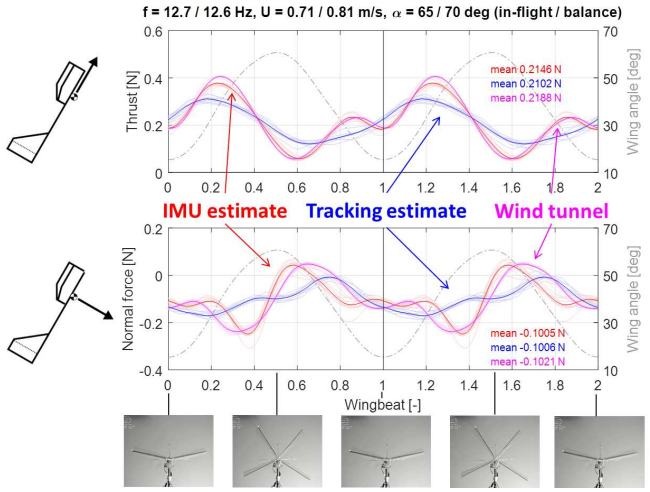

Fig. 7. A comparison of steady state in-flight forces estimated with IMU and external motion tracking based data. Wind tunnel forces measured at similar conditions are shown for reference. All the data is low-pass filtered (4th order Butterworth zero-phase filter, 40 Hz cut-off frequency) [21].

IV. Fusion of External Motion Tracking and On-Board IMU Data

In some cases, both optical tracking and on-board data acquisition systems are available simultaneously, and this may be exploited to obtain more reliable and informative data.

Optical tracking systems [9], [17], [30] yield reliable position measurements, whose accuracy is undiminished over time, but they entail a number of limitations (cf. Sec. II): *i)* the currently available systems typically have a relatively low bandwidth, which may be insufficient to analyze sub-flap processes; *ii)* glitches and untracked or fused markers may occur, see Sec. II-B ; *iii)* velocities and accelerations need to be computed via numerical differentiation, which leads to increased noise and loss of information, cf. Sec.II-F [19]; *iv)* for increasingly small platforms, the attitude measurements obtained from tracking deteriorate in quality due to the limited resolution – which is likely to become an increasingly relevant problem given the trend to develop smaller FW-MAVs. On-board data acquisition systems typically consist of IMU sensors (cf. Sec. III), which can have high bandwidth, allowing for higher-frequency measurements, and directly provide angular velocity and acceleration measurements that are accurate for short times. Unlike optical tracking, these sensors are not inherently affected by vehicle size. Drawbacks of these sensors include significant measurement noise, biases and integration drift (when they are used to determine attitude, velocity or position). In this section we outline an approach to combine the two previously presented data acquisition methods effectively, specifically for flapping-wing modeling and analysis, avoiding some of the aforementioned limitations. Further details can be found in [22].

1) Time synchronization: The first step in combining two data acquisition sources is to ensure time synchronization. A simple approach to do this [21] is to take advantage of the LED markers used for tracking, by having a marker switch on and off when the on-board logging starts and ends. This method may still leave a small residual time shift (in our experience typically in the order of milliseconds) that can be removed by considering the time-resolved component of one of the measurements. By shifting the on-board estimate in both directions until the error between it and the corresponding off-board measurement (resampled to the same rate) is minimized, the remaining time shift can be computed and used to synchronize all the data more accurately. The measurement used for this detailed alignment should be selected depending on the platform and experimental setup. It is advisable to select the most reliable measurement (cf. Sec. III-A), and containing the least external influence, e.g., dynamic excitation. Alternatively, time synchronization can be included implicitly in the sensor fusion method by means of multi-rate fusion filters that account for different sampling rates and are updated whenever one of the data acquisition sources provides a new measurement [31], [32].

2) Sensor fusion: Once the measurements have been synchronized, they can be fused. An extended Kalman filter (EKF) was found to provide effective results [22], while being straightforward to implement. By suitable tuning of the measurement and process noise matrices it becomes possible to achieve accurate estimates for both the slow dynamics over long time scales, and the short-term fast dynamics. The typically available tracking and on-board data acquisition systems allow for estimation of the body attitude and velocity, as well as of the IMU sensor biases. A standard EKF can be used for this, with IMU accelerometer and gyroscope data as input variables and optical tracking data as output measurements [22], resulting in the following filter definition and equations:

States (x), inputs (u), outputs (z), process noise (w), measurement noise (v):

$$x = [\Phi\ \Theta\ \Psi\ u_b\ v_b\ w_b\ b_p\ b_q\ b_r\ b_{ax}\ b_{ay}\ b_{az}]^T \quad (15)$$

$$u = [p\ q\ r\ a_x\ a_y\ a_z]^T \quad (16)$$

$$z = [\Phi_m\ \Theta_m\ \Psi_m\ u_b\ v_b\ w_b]^T \quad (17)$$

$$v = [v_\Phi\ v_\Theta\ v_\Psi\ v_{ub}\ v_{vb}\ v_{wb}]^T \quad (18)$$

$$w = [w_p\ w_q\ w_r\ w_{ax}\ w_{ay}\ w_{az}]^T \quad (19)$$

Process equations:

$$\dot{\Phi} = (p-b_p)+(q-b_q)s\Phi\tan\Theta+(r-b_r)\cos\Phi\tan\Theta \quad (20)$$
$$\dot{\Theta} = (q-b_q)\cos\Phi-(r-b_r)s\Phi \quad (21)$$
$$\dot{\Psi} = (q-b_q)s\Phi\sec\Theta+(r-b_r)\cos\Phi\sec\Theta \quad (22)$$
$$\dot{u}_B = (r-b_r)v_b-(q-b_q)w_b-gs\Theta+a_x-b_{ax} \quad (23)$$
$$\dot{v}_B = -(r-b_r)u_b+(p-b_p)w_b+gs\Phi\cos\Theta+a_y-b_{ay} \quad (24)$$
$$\dot{w}_B = (q-b_q)u_b-(p-b_p)v_b+g\cos\Phi\cos\Theta+a_z-b_{az} \quad (25)$$
$$\dot{b}_p = 0; \quad \dot{b}_q=0; \quad \dot{b}_r=0 \quad (26)$$
$$\dot{b}_{ax} = 0; \quad \dot{b}_{ay}=0; \quad \dot{b}_{az}=0 \quad (27)$$

Measurement equations:

$$\Phi_m = \Phi+v_\Phi \quad (28)$$
$$\Theta_m = \Theta+v_\Theta \quad (29)$$
$$\Psi_m = \Psi+v_\Psi \quad (30)$$
$$u_{b,m} = u_b+v_{ub} \quad (31)$$
$$v_{b,m} = v_b+v_{vb} \quad (32)$$
$$w_{b,m} = w_b+v_{wb}, \quad (33)$$

where (Φ,Θ,Ψ) are the Euler angles, (p,q,r) are the roll, pitch and yaw rates, (u_b,v_b,w_b) are the body-frame velocities, (a_x,a_y,a_z) are the accelerometer-measured accelerations, $(b_p,b_q,b_r,b_{ax},b_{ay},b_{az})$ are the sensor biases of the gyroscope and accelerometer, $(v_{ub},v_{vb},v_{wb},v_\Phi,v_\Theta,v_\Psi)$ are the measurement noise in the measured velocities and attitudes, and $(w_p,w_q,w_r,w_{ax},w_{ay},w_{az})$ are the process noise in the rates and accelerations. The subscript m denotes measurements. If, as is often the case, no direct velocity measurement is available, the required filter inputs must be computed by differentiating the tracking positions. This may decrease the quality of the final result.

The central step in designing the filter is the definition of the process and measurement noise covariance matrices, Q and R. The initial tuning can be based on the actual noise characteristics of already available measurements, while further adjustments can then be made to improve the result, in an iterative process. Considering the typical properties of on-board and off-board data acquisition systems, mentioned earlier, a desirable result may be one where the IMU data *i)* ensure a sufficiently high frequency content, *ii)* compensate for occasional tracking errors, and *iii)* increase the information content and reliability of the rates and accelerations thanks to their direct measurement; while the optical tracking is used as a basis especially for the slower and long-term changes.

As a result, to obtain extensive high-frequency information, more weight can be given to the on-board measurements, by scaling down the R matrix to values smaller than suggested by analysis of the noise characteristics of the tracking data. Similarly, the Q matrix may be scaled to somewhat larger values, reducing the confidence in the on-board data. This additional scaling can be used to achieve the desired balance between the two data sources. At the same time it is important to ensure that the final result remains realistic and that suitable filter properties are obtained. While the tuning involves experimental testing and visual assessment to evaluate to what extent the desired outcome is achieved, there are ways to guide this process. One possibility is to consider the properties of the resulting filter, for instance comparing the innovation errors to the uncertainty bounds predicted by the EKF. The tuning should be such that the innovation errors are small and the filter convergence times sufficiently short while, at the same time, avoiding significant discrepancies between estimated error bounds and computed innovation errors. Further details on the tuning and filter design process can be found in [22].

3) State estimation results: Fig. 8 shows an example of longitudinal states (horizontal and vertical velocities and pitch attitude) obtained through the proposed EKF-based fusion of IMU and optical tracking data, compared to the corresponding data calculated from the tracking measurements and from the IMU. It can be remarked that considerable agreement is obtained between tracking and fused data, while at the same time the high-frequency component contains more information thanks to the on-board data. In addition to the general advantages of sensor fusion, e.g. compensating for sensor drift and increasing the overall reliability, the available level of detail is thus increased. Moreover, loss of information due to numerical differentiation is countered.

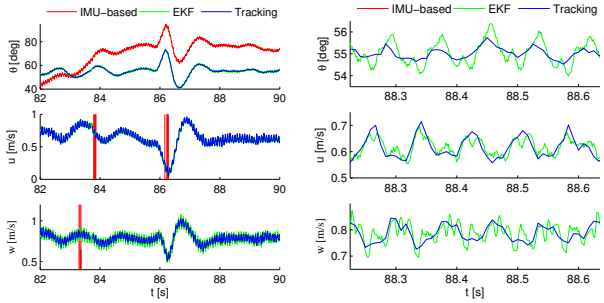

(a) (b)

Fig. 8. Example of pitch attitude and vertical and horizontal velocities obtained via IMU/tracking data fusion (EKF); at increasingly small time scale from (a) to (b). Note that in (b) the IMU-based states (red) move outside the axis range, and are not visible on the plot.

V. FLIGHT TESTING

A. Identification maneuvers/ input design

Input design is a key element in the system identification process, ensuring that the collected data contain sufficient and useful information to allow for models to be extracted from them. Inputs for system identification must excite the dynamics of the system in the range of interest, while remaining compatible with the constraints dictated by the available experimental setup and possibly the modeling approach. Input design has been studied extensively for standard aerospace applications, especially fixed-wing ones. However, novel systems like FWMAVs still constitute a challenge due to their high complexity, the more limited knowledge we have of them, and the limited flight experience and data available. This section summarizes a number of

recommendations/guidelines for input design, specifically for small flapping-wing vehicles, based on our flight testing experience, as well as preliminary studies [9], [17], [20], [33].

Firstly, the type of input must be selected. Inputs that are somehow optimized [23], [34], [35] may provide effective results, however they typically require extensive prior knowledge of the system and are complex to design and implement. Given the complexity of flapping-wing vehicles and the difficulties and limitations involved in the flight testing process, this approach is not recommended as a starting point, particularly for new platforms.

If a system is not well known, an attractive solution is given by frequency sweeps, designed to cover a wide range of frequencies, so that accurate prior knowledge of the system dynamics is dispensable. The drawback is that these inputs have relatively long durations if a wide frequency band is to be covered – this is particularly problematic when the flight space is limited, as is typically the case for indoor testing of MAVs. An additional drawback is the inability of these signals to excite several axes simultaneously, which limits the possibility of modeling coupled dynamics.

When a new vehicle is tested, a straightforward but effective approach is the use of multi-step inputs, such as doublets, 211 or 3211 signals. These can be easily programmed and executed, are relatively rapid, can be used to excite several axes simultaneously if applied to different actuators in sequence, and can be tailored to the system and setup with relative ease, even when the dynamics are not yet well known. Through extensive flight testing we found such signals to provide suitable excitation, while presenting fewer challenges than frequency seep [17], [20].

It is worth noting, however, that multi-step inputs range from simple doublets to more advanced combinations of pulses, such as 211 or 3211 signals. The latter can excite a somewhat wider range of frequencies, however they involve longer execution times. This can be a problem when flight space - hence time – is limited, particularly when the platform dynamics are fast, which is often the case for highly maneuverable flapping-wing flyers. These signals are also asymmetric, which, as mentioned above, can be a limitation. In view of this, doublets are considered the most effective solution in a typical flapping-wing flight testing setup, at least to start with. They are simple to execute, even manually, relatively simple to design, rapid compared to 211 and 3211 inputs, and symmetrical, which is advantageous if linear modeling approaches are to be applied, as the vehicle is more likely to remain close to its initial steady flight condition following the excitation.

Furthermore, multi-step inputs must be tuned, based on a number of considerations, some unique to the flapping-wing case. Firstly, the signal must provide sufficient excitation. A longer and larger input leads to more information but also requires more time and is unsuitable for linear modeling approaches. By contrast, small, rapid inputs entail unclear responses and significant noise influence. These problems can be accentuated in the flapping-wing case, where, depending on the flapping frequency, the flapping motion can introduce considerable body oscillations, that one may not wish to consider when modeling the dynamics.

Related to this, an additional requirement may be that the input must allow the body dynamics to be distinguishable from the flapping effects. In many studies, sub-flap cycle effects are neglected when dealing with the dynamics: in this case, the flapping-related oscillations can be considered a disturbance, which may lead to a low signal-to-noise ratio and adversely affect the identification process. Such oscillations may be significant and the effect may have to be countered using additional low-pass filtering [17], [20] or larger than usual input signals [20] - the former is preferable when linear models are used, as the latter may conflict with possible linearity requirements.

Additional restrictions are imposed by the typically limited flight space used with flapping-wing vehicles, when optical tracking is employed. This implies that limited time is available for each maneuver, which may lead to parts of the dynamics not being captured effectively in the data, resulting in more variation in the identified dynamics. Moreover, the edge of the flight space is reached rapidly, requiring frequent sharp turns and subsequently additional time to return the vehicle to the steady state condition. Spacial restrictions must be considered when designing the input signal, to ensure that the result is attainable.

The detailed design process is somewhat iterative, as many different requirements must be considered. If any information is available on the platform, an approximate duration for the signal [36] can be derived from frequency-domain analysis, such that the power content is highest around the expected natural frequency. Similar vehicles can be used to provide initial tentative values for entirely new platforms. Further adjustments may then be required to account for the aforementioned restrictions in the experimental setup, and a better result can be obtained through iterative adjustments once more information on the vehicle becomes available in the testing process. Adjustments may also be necessary depending on the particular flight condition, e.g., if some of the actuators are also used to maintain a specific flight condition, less maneuvering space remains available for excitation. Moreover, it should be considered that the vehicle dynamics are likely to vary in different flight conditions (e.g., hover versus forward flight), by adjusting the input amplitude if a more aggressive response is anticipated.

Once an input signal has been designed, it can either be applied manually or pre-programmed and applied automatically by an autopilot. The latter option allows for higher maneuver complexity and improved repeatability, and is often preferable especially for small and/or unusual vehicles, which are more difficult to fly manually.

It should be noted that while our observations are based on testing of tailed flapping-wing MAVs, similar procedures can be applied to tailless platforms – due to their inherent

instability, these need to be tested as closed loop systems.

VI. Conclusions

This article addressed the most important aspects to consider when performing flight tests with flapping-wing micro aerial vehicles (FWMAV), using external motion tracking systems, on-board sensors and sensor fusion, for system identification and modeling purposes. In terms of requirements, the FWMAV should be equipped with retro-reflective markers or, preferably, infra-red LEDs, with no symmetry plane between them; the external tracking system should be capable of delivering a resolution that allows for the accurate flight path reconstruction at the desired flight speeds. On-board sensors, e.g., inertial measurement unit, should be placed close to the center of mass of the robot. Such sensors, with data logging or down-link capability, can increase the overall precision and reliability of the data, and provide more information at smaller time scales, particularly through sensor fusion with external tracking data, using, for instance, an extended Kalman filter scheme. Special attention should be drawn to data post-processing, as it can severely impact the quality of the information in the data. Provided that the sampling frequency of the tracking system is at least five times higher than the mode one wants to capture, three-point central difference differentiation schemes are recommended to compute the velocity and acceleration flight states. In other cases, on-board sensors (and sensor fusion) or differentiation in the frequency domain is advised. Furthermore, the flight test maneuvers should be designed to excite the dynamic modes of the FWMAV, and executed in such a way that repeatability and input precision are ensured. Therefore, it is recommended that the maneuvers are programmed in the autopilot, whenever possible. For force reconstruction, simple single rigid body equations of motion, know as, aircraft equations of motion, are sufficient to determine the forces and moments that act in free-flight. Alternatively, and when possible, the forces can be reconstructed effectively using on-board sensors only.

References

[1] T. Weis-Fogh, "Energetics of hovering flight in hummingbirds and in drosophila," *Journal of Experimental Biology*, vol. 56, pp. 79–104, February 1972.

[2] C. P. Ellington, "The aerodynamics of hovering insect flight. I. The quasi-steady analysis," *Philosophical Transactions of the Royal Society of London. Series B, Biological Sciences*, vol. 305, no. 1122, pp. 1–15, 1984.

[3] R. A. Norberg, "The pterostigma of insect wings an inertial regulator of wing pitch," *Journal of Comparative Physiology*, vol. 81, no. 1, pp. 9–22, 1972.

[4] L. Bennett, "Clap and fling aerodynamics-an experimental evaluation," *Journal of Experimental Biology*, vol. 69, no. 1, pp. 261–272, 1977.

[5] G. R. Spedding and T. Maxworthy, "The generation of circulation and lift in a rigid two-dimensional fling," *Journal of Fluid Mechanics*, vol. 165, pp. 247–272, 4 1986.

[6] S. Sunada, K. Kawachi, I. Watanabe, and A. Azuma, "Fundamental analysis of three-dimensional 'near fling'," *Journal of Experimental Biology*, vol. 183, no. 1, pp. 217–248, 1993.

[7] R. J. Wood, "The first takeoff of a biologically-inspired at-scale robotic insect," *IEEE Tranactions on Robotics*, vol. 24(2), pp. 341–347, 2008.

[8] S. S. Baek and R. S. Fearing, "Flight forces and altitude regulation of 12 gram i-bird," in *IEEE RAS and EMBS International Conference on Biomedical Robotics and Biomechatronics (BioRob)*, pp. 454–460, 2010.

[9] J. Grauer, E. Ulrich, J. H. Jr., D. Pines, , and J. S. Humbert, "Testing and system identification of an ornithopter in longitudinal flight," *Journal of Aircraft*, vol. 48, pp. 660–667, March-April 2011.

[10] J. V. Caetano, C. C. de Visser, G. C. H. E. de Croon, B. D. W. Remes, C. de Wagter, J. L. Verboom, and M. Mulder, "Linear Aerodynamic Model Identification of a Flapping Wing MAV Based on Flight Test Data," *International Journal of Micro Air Vehicles*, vol. 5, pp. 273–286, December 2013.

[11] K. Ma, P. Chirarattananon, S. B. Fuller, and R. J. Wood, "Controlled flight of a biologically inspired, insect-scale robot," *Science*, vol. 340, no. 6132, pp. 603–607, 2013.

[12] S. F. Armanini, C. C. de Visser, G. C. H. E. de Croon, and M. Mulder, "Time-Varying Model Identification of Flapping-Wing Vehicle Dynamics Using Flight Data," *Journal of Guidance, Control, and Dynamics*, vol. 39, no. 3, 2016.

[13] R. Y. Krashanitsa, D. Silin, and S. V. Shkarayev, "Flight dynamics of flapping-wing air vehicle," in *Atmospheric Flight Mechanics Conference,*, 2008-6698, AIAA, August 2008.

[14] M. Percin, B. van Oudheusden, H. Eisma, and B. Remes, "Three-dimensional vortex wake structure of a flapping-wing micro aerial vehicle in forward flight configuration," *Experiments in Fluids*, vol. 55, no. 9, 2014.

[15] B. F. Mettler, "Extracting micro air vehicles aerodynamic forces and coefficients in free flight using visual motion tracking techniques," *Exp. Fluids*, vol. 49, pp. 557–569, 2010.

[16] G. Lim, S. Shkarayev, Z. Goff, and P. Beran, "Studies of flight kinematics of ornithopters," in *International Competition and Conference on Micro Air Vehicles*, IMAV 2012, 2012.

[17] J. V. Caetano, C. C. de Visser, B. D. W. Remes, C. de Wagter, and M. Mulder, "Controlled flight maneuvers of a Flapping Wing Micro Air Vehicle: a step towards the DelFly II Identification," in *AIAA Atmospheric Flight Mechanics Conference*, no. 2013-4843, 2013.

[18] M. Karasek, A. Hua, Y. Nan, M. Lalami, and A. Preumont, "Pitch and roll control mechanism for a hovering flapping wing mav," *International Journal of Micro Air Vehicles*, vol. 6, pp. 253–264, December 2014.

[19] J. V. Caetano, M. Percin, B. W. van Oudheusden, B. D. W. Remes, C. de Wagter, G. C. H. E. de Croon, and C. C. de Visser, "Error Analysis and Assessment of Unsteady Forces Acting on a Flapping Wing Micro Air Vehicle: Free-Flight versus Wind Tunnel Experimental Methods," *Bioinspiration & Biomimetics*, vol. 10, no. 5, 2015.

[20] S. F. Armanini, M. Karásek, C. C. de Visser, G. C. H. E. de Croon, and M. Mulder, "Flight testing and preliminary analysis for global system identification of ornithopter dynamics using on-board and off-board data," in *AIAA Atmospheric Flight Mechanics Conference*, 2017.

[21] M. Karásek, A. J. Koopmans, S. F. Armanini, B. D. W. Remes, and G. C. H. E. de Croon, "Free flight force estimation of a 23.5 g flapping wing MAV using an on-board IMU," in *The 2016 IEEE/RSJ International Conference on Intelligent Robots and Systems (IROS 2016), Daejeon, Korea, 9-14 October 2016 (Accepted]*, 2016.

[22] S. F. Armanini, M. Karásek, d. G. C. H. E., and C. C. de Visser, "Onboard/ offboard sensor fusion for high-fidelity flapping-wing robot flight data," *Journal of Guidance, Control and Dynamics*.

[23] J. A. Mulder, *Design and evaluation of dynamic flight test manoeuvers*. PhD thesis, Deft University of Tecnhology, 1986.

[24] P. J. Brockwell and R. A. Davis, *Time Series: Theory and Methods*. Springer, second ed., 2006. ISBN 0-387-97429-5.

[25] G. E. P. Box, G. M. Jenkins, and G. C. Reinsel, *Time Series Analysis: Forecasting and Control*. Wiley, fourth ed., 2008. ISBN 978-0-470-27284-8.

[26] G. Bohm and G. Zech, *Introduction to Statistics and Data Analysis for Physicists*. DESY, 1 ed., 2010. ISBN: 3935702418.

[27] P. R. Bevington and D. K. Robinson, *Data Reduction and Error Analysis for the Physical Sciences*. New York, NY: McGraw-Hill, third ed., 2003. ISBN 0-07-247227-8.

[28] A. E. Marble, S. Member, and C. M. M. C. Intyre, "Comparison of Digital Algorithms Used in Computing the Derivative of Left Ventricular Pressure," no. 7, pp. 524–529, 1981.

[29] T. S. Yoo, S. K. Hong, H. M. Yoon, and S. Park, "Gain-Scheduled Complementary Filter Design for a MEMS Based Attitude and Heading Reference System," *Sensors*, vol. 11, pp. 3816–3830, mar 2011.
[30] P. Chirarattananon and R. J. Wood, "Identification of flight aerodynamics for flapping-wing microrobots," in *IEEE International Conference on Robotics and Automation (ICRA)*, pp. 1381–1388, IEEE, 2013.
[31] L. P. Yan, B. S. Liu, and D. H. Zhou, "The modeling and estimation of asynchronous multirate multisensor dynamic systems," *Aerospace Science and Technology*, vol. 10, pp. 63–71, 2006.
[32] F. Caron, E. Duflos, D. Pomorski, and P. Vanheeghe, "Gps/imu data fusion using multisensor kalman filtering: introduction of contextual aspects," *Journal of Information Fusion*, p. 221230, 2004.
[33] S. S. Baek, "Autonomous ornithopter flight with sensor-based behavior," *Univ. California, Berkeley, Tech. Rep. UCB/EECS-2011-65*, 2011.
[34] E. Plaetschke and G. Schulz, "Practical input signal design," in *Parameter Identification AGARD-LS-104*, NATO, 1979.
[35] E. A. Morelli and V. Klein, "Optimal input design for aircraft parameter estimation using dynamic programming principles," in *AIAA Atmospheric Flight Mechanics Conference*, (Portland,), AIAA, August 1990.
[36] R. Jategaonkar, *Flight Vehicle System Identification A Time Domain Methodology*. Reston, VA, USA: AIAA Progress in Astronautics and Aeronautics, 2006.